Synoptic Climatology of Rain-on-Snow Events in Alaska

ALEX D. CRAWFORD, KAREN E. ALLEY, AND ANNA M. COOKE

Department of Earth Sciences, The College of Wooster, Wooster, Ohio

MARK C. SERREZE

National Snow and Ice Data Center, Cooperative Institute for Research in Environmental Sciences, University of Colorado Boulder, Boulder, Colorado

(Manuscript received 20 September 2019, in final form 30 December 2019)

ABSTRACT

Rain-on-snow (ROS) events can have adverse impacts on high-latitude ungulate populations when rain freezes in the snowpack, forming ice layers that block access to winter forage. In extreme cases, ROS events have led to mass die-offs. ROS events are linked to advection of warm and moist air, associated with extratropical cyclones. However, these conditions are common to many winter precipitation events, challenging our understanding of the particular conditions under which ROS events occur. This study uses the Modern-Era Retrospective Analysis for Research and Applications version 2 (MERRA-2) to differentiate ROS events in Alaska from precipitation events in which only snow falls on a preexisting snowpack [snow-on-snow (SOS)]. Over the North Slope and Kotzebue Sound, no clear difference exists between the tracks of ROS-producing and SOS-producing storms. However, in the interior, southwest, and Anchorage, tracks of ROS-producing storms tend to be farther north and west than for SOS-producing storms. The northwest shift of ROS-producing storms is linked to the position of upper-tropospheric anticyclones in the eastern Gulf of Alaska during ROS events. ROS-producing storms are no more intense than SOS-producing storms, but their association with atmospheric blocking leads to stronger pressure gradients on the east side of storms and thereby stronger advection of positive anomalies in temperature and precipitable water. For several sites, sea level pressure in the eastern Gulf of Alaska is also significantly higher a few days prior to ROS events than prior to SOS events, further implicating atmospheric blocking as a facilitator and potential predictor of ROS events.

1. Background and motivation

Rain falling on a preexisting snowpack [rain-on-snow (ROS)] can have cascading impacts. As rain percolates through the snowpack, it may freeze, releasing latent heat that can rapidly warm the snow (Conway and Benedict 1994). In some cases, the influx of liquid water is sufficient to destabilize the snowpack and cause avalanches (Conway and Raymond 1993; Hansen et al. 2014; Stimberis and Rubin 2017), early snowmelt onset (Semmens et al. 2013), or flooding (McCabe et al. 2007; Freudiger et al. 2014; Il Jeong and Sushama 2018). When freezing occurs along the snow–soil interface, it can hold upper soil temperatures at 0°C and degrade permafrost (Putkonen and Roe 2003; Rennert et al. 2009; Hansen et al. 2014).

An important ecological impact of ROS events is the blocking or impeding of forage access for ungulates like reindeer, caribou, elk, and musk ox due to formation of ice layers on the ground or within the snowpack (e.g., Miller et al. 1975; Reimers 1982; Aanes et al. 2000). In response to a widespread ROS event in October 2003, the Teshekpuk caribou herd in Alaska migrated 400 km east for easier forage (Brown 2005). Reindeer may also employ selective cratering (digging through the snowpack for forage), such as in Sarsøyra, Svalbard, in 2005–06 when reindeer sought windblown ridges and higher elevations that were ice free although they had sparser

Supplemental information related to this paper is available at the Journals Online website: https://doi.org/10.1175/MWR-D-19-0311.s1.

Corresponding author: Alex D. Crawford, acrawford@wooster.edu

DOI: 10.1175/MWR-D-19-0311.1

vegetation (Hansen et al. 2010). However, these tactics can be energy intensive, and ungulates may still succumb to starvation. The Teshekpuk herd suffered 25% mortality from 2003 to 2004 (Brown 2005; Bieniek et al. 2018), and reindeer at Sarsøyra suffered 23.6% mortality from 2005 to 2006 (Hansen et al. 2010). Moreover, several studies have demonstrated a negative correlation between the amount of winter rain (or more specifically ROS) and population growth of Svalbard reindeer (Aanes et al. 2000; Kohler and Aanes 2004; Hansen et al. 2011). Other recent mass die-offs linked to ROS events have occurred on Banks Island in the Canadian Arctic Archipelago in 2003 (Rennert et al. 2009), northern Quebec in 2010 (Dolant et al. 2016), Svalbard in 2012 (Hansen et al. 2014), and on the Yamal Peninsula of Siberia in 2006 and 2013 (Forbes et al. 2016).

ROS is most common in places like Iceland, Norway, and southern Alaska, which have wet climates and can experience both snow and rain during winter months (Rennert et al. 2009; Cohen et al. 2015). ROS in Alaska is generally most common in the early and late cold season (e.g., October and April), when a snowpack is present but rain is more likely to occur (Bieniek et al. 2018; Pan et al. 2018). The North Slope is an exception to this seasonality, experiencing ROS in October, but not in March or April (Bieniek et al. 2018). Ecological impacts of ROS events vary based on the time of year and the persistence of ice in the snowpack. Early season ROS events, for instance, are most dangerous to caribou because any ice that is formed can persist throughout winter (Rennert et al. 2009). Expected temperature increases in coming decades will shorten the Alaskan snow season (Littell et al. 2018) but increase the likelihood of rain events during the snow season (Bieniek et al. 2018). Therefore, trends in ROS events as the climate warms are likely to vary by region. Increasing frequency is projected in many areas, especially at higher latitudes (Rennert et al. 2009; Cohen et al. 2015) such as along the North Slope (Bieniek et al. 2018).

ROS events tend to occur during warm-air incursions with positive anomalies in precipitable water (column-integrated water vapor) (Rennert et al. 2009; Forbes et al. 2016; Pan et al. 2018). In Alaska, the heaviest rainfalls from ROS events are typically associated with a strong high pressure system to the east and a strong low to the west of the ROS location (Bieniek et al. 2018). ROS frequency in Svalbard, by comparison, is positively correlated with the North Atlantic Oscillation (NAO) index because when the NAO is positive, more extratropical cyclones track toward Svalbard, directing warm air and atmospheric moisture northward (Putkonen and Roe 2003). Similar connections have been observed for ROS events and the NAO/Arctic Oscillation in northern Europe (Cohen et al. 2015; Pall et al. 2019) and European Russia (Ye et al. 2008) and between ROS and the Pacific–North America (PNA) pattern in the Canadian Arctic Archipelago (Rennert et al. 2009).

While much has been learned about ROS events over the past decade, an ongoing challenge to furthering our understanding is that conditions associated with ROS events (advection of warm and moist air linked to the passage of extratropical cyclones) can be similar to events that only produce snow falling on an existing snowpack [snow-on-snow (SOS)]. The present paper addresses this challenge for the state of Alaska, a large and economically important region with a diversity of environments, from coastal to interior, and from temperate to Arctic. Our study is guided by three research questions:

1) Do storms that produce ROS have distinct tracking histories from those that produce SOS?
2) Are large-scale circulation patterns during ROS events different from those during SOS events?
3) Are large-scale circulation patterns in the days leading up to a precipitation event (e.g., 72 or 120 h before) different for ROS versus SOS?

Using data from version 2 of the Modern-Era Retrospective Analysis for Research and Applications (MERRA-2; Gelaro et al. 2017), synoptic-scale cyclones are catalogued using a Lagrangian detection and tracking algorithm (Crawford and Serreze 2016) applied to sea level pressure (SLP) fields. We also compare atmospheric conditions during and leading up to ROS and SOS events at several locations throughout the state, selected to represent the variety of Alaskan environments and based on the availability of reliable surface data (for validation) during the MERRA-2 period (Fig. 1). By distinguishing between ROS and SOS events, we are able to refine descriptions of storm behaviors and conditions leading to ROS events. Because of their greater potential for adverse impacts on ungulates, particular attention is paid to ROS events that are followed by prolonged subfreezing temperatures.

2. Data and methods

a. Overview

Detection of ROS events requires knowledge of 1) the presence of an existing snowpack and 2) precipitation falling in the form of rain. Data sources for ROS detection used in past studies include direct surface observations (e.g., Pall et al. 2019), output from atmospheric reanalyses (e.g., Rennert et al. 2009; Hansen et al. 2014; Cohen et al. 2015; Bieniek et al. 2018), and

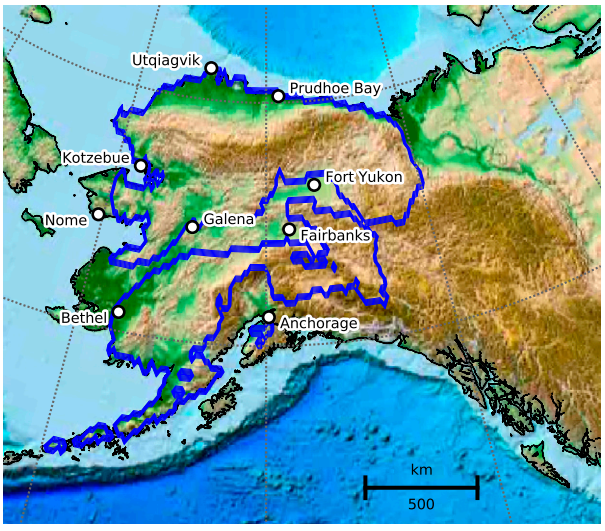

FIG. 1. Study area showing Alaskan topography (NOAA's ETOPO1; https://www.ngdc.noaa.gov/mgg/global/), the range of Alaskan caribou herds (blue outline; https://www.adfg.alaska.gov/index.cfm?adfg=caribou.main), and the locations of focus for this study.

satellite observations of liquid water and ice formation in the snowpack via microwave backscatter (Wilson et al. 2013) or microwave emission (Dolant et al. 2016; Langlois et al. 2017; Pan et al. 2018). Some past studies have assumed the presence of snow, classifying any rain event in winter months as a potential ROS event (e.g., Putkonen and Roe 2003; Hansen et al. 2014). However, most studies have incorporated some minimum snow depth or snow-water equivalent and minimum rainfall total for identifying ROS (e.g., Rennert et al. 2009; Cohen et al. 2015; Bieniek et al. 2018; Pall et al. 2019). A few studies have further refined the events being detected. For example, snowpack mass change following ROS events has been used to assess impacts on flooding (McCabe et al. 2007; Il Jeong and Sushama 2018), while measurement of liquid water in the snowpack followed by freezing regardless of whether precipitation occurred (Wilson et al. 2013; Pan et al. 2018) has been used to assess impacts on ungulates. Bieniek et al. (2018) expanded their detection to include rain falling on frozen ground, which can also inhibit foraging.

Our approach for detecting and diagnosing ROS events using MERRA-2 is similar to past reanalysis-based studies, although we use hourly rather than daily output to define events. To contrast the synoptic conditions associated with SOS and ROS, events are related to cyclone tracks from a database using MERRA-2 SLP fields, developed as part of previous studies (Crawford and Serreze 2016, 2017).

b. MERRA-2

Variables acquired from MERRA-2 include gauge-adjusted precipitation and snowfall, snow depth, skin temperature, 2-m air temperature, SLP, geopotential height at 500 hPa (GPH), and precipitable water for the years 1980–2018. Data were acquired at a 0.5° latitude by 0.5° longitude spatial resolution and an hourly temporal resolution for all months. The hourly temporal resolution is particularly valuable for linking specific ROS events to individual storms.

MERRA-2 has more sophisticated corrections for land precipitation (Reichle et al. 2017b), better overall treatment of snow cover (Reichle et al. 2017a), and fewer heterogeneities from changes in the observing system (Gelaro et al. 2017) than its MERRA predecessor. However, because direct precipitation observations at high latitude are sparse and have their own biases, bias correction to precipitation output from MERRA-2 is only performed south of 62.5°N (Reichle et al. 2017b). To the extent that high-latitude gauge measurements can be trusted, there is a positive bias for MERRA-2 precipitation (especially in summer; Reichle et al. 2017b) and snow cover (Reichle et al. 2017a) over much of Alaska. Overly frequent precipitation is a common bias in all reanalyses, but MERRA-2 has an especially large fraction of precipitation coming from trace precipitation events (Boisvert et al. 2018). Steps taken to mitigate this problem are outlined shortly.

Additional validation of MERRA-2 was performed for this study by comparing year-round precipitation, snow depth, and temperature values to daily observations from ten weather stations that are part of the Global Historical Climatology Network (GHCN; Menne et al. 2012), including the nine locations marked in Fig. 1 and five of the six stations highlighted by Bieniek et al. (2018) in their discussion section. MERRA-2 has a known positive snow bias (Reichle et al. 2017a), and comparison of MERRA-2 output to these direct observations confirms overestimation of snow cover at all stations (Table 1). Even when "snow cover presence" in MERRA-2 is defined as a grid cell with a snow depth of at least 25.4 mm (1 in.), MERRA-2 captures 95%–100% of the days with nonzero snow cover in the GHCN records. Moreover, a median of 81.6% of days with at least 25.4 mm of snow depth in MERRA-2 had snow cover recorded in the GHCN record. MERRA-2 also records excessive low (<2.54 mm) and trace precipitation events (Fig. 2). Based on these comparisons, minimum precipitation and snow depth thresholds were used for ROS identification with MERRA-2 data (see following section). This mitigates the potential for overcounting ROS events. Comparisons to GHCN data also confirmed that

TABLE 1. Comparison of days with snow cover recorded at nine study locations in Alaska based on GHCN and MERRA-2. "Snow cover" is defined as a nonzero snow depth or snow-water equivalent for GHCN and a gridcell snow depth greater than 25.4 mm (1 in.) for MERRA-2.

	Bethel	Anchorage	Galena	Fairbanks	Fort Yukon	Nome	Kotzebue	Utqiaġvik	Prudhoe Bay
No. of days with snow cover in GHCN	161	155	204	194	306	193	161	254	261
% of those days with snow cover in MERRA-2	99.8	100.0	99.9	99.8	95.1	99.7	99.3	99.7	99.8
No. of days with snow cover in MERRA-2	221	222	235	225	304	235	249	318	328
% of those days with snow cover in GHCN	72.4	69.8	86.7	86.1	95.7	81.6	85.5	79.6	79.3

MERRA-2 does not share the cold-rain bias observed by Bieniek et al. (2018) in daily data from the ECMWF interim reanalysis (ERA-I; Fig. S1 in the online supplemental material). Additionally, hourly observations from these same stations, available for some years, were used to validate the average length of precipitation events being identified.

The results from this study must be viewed with the caveat that ROS and SOS events are identified using a single atmospheric reanalysis. Partitioning between rain and snow may vary by reanalysis, as may the amount of precipitation associated with individual events. However, the relationships shown appear to be physically robust, which supports the validity of conclusions drawn from this study.

c. *ROS and SOS identification*

For every MERRA-2 grid cell that intersects with Alaskan land (including islands), a precipitation event was defined as a set of hours with MERRA-2 precipitation of at least 0.254 mm h^{-1}, which matches the minimum recorded precipitation in the GHCN records (0.01 in.). Following Yu et al. (2007), we defined precipitation events to have temporal gaps of no more than 1 h for which the precipitation rate falls below this threshold. Total precipitation, snowfall, and rainfall were recorded for each event, along with event length, the maximum and minimum 2-m air temperature and skin temperature during the event, and the starting and ending snow depth.

Next, ROS events were identified as any precipitation event meeting the following criteria:

1) Total rainfall is at least 2.54 mm (0.1 in.).
2) Snow depth exceeds 25.4 mm (1 in.) at both the start and end of the event.

Requiring snow to persist through the event identifies those ROS events that may lead to icing and therefore inhibit foraging. The snow depth threshold is higher than used in past studies (e.g., Rennert et al. 2009; Bieniek et al. 2018) to adjust for the positive snow-cover bias in MERRA-2 (Fig. S1; Reichle et al. 2017a). A rainfall minimum of 2.54 mm is used rather than the 0.254 mm used by Bieniek et al. (2018) because MERRA-2 is in better agreement with surface observations for days with precipitation exceeding 2.54 mm, although still biased high (Fig. 2). Similarly, the snow depth requirement mitigates the positive snow bias in MERRA-2 (Table 1). A subclass of ROS events was identified using an additional criterion:

3) At least 95% of the subsequent 720 h (30 days) have skin temperatures at or below 0°C.

This highlights ROS events that have an increased chance of adversely impacting foraging because they are followed by prolonged freezing (hereafter called ROSF events).

SOS events are identified as events for which only snow falls on a preexisting snowpack: total precipitation $\geq$2.54 mm; total rainfall $<$0.254 mm; snow depth $>$25.4 mm. Therefore, mixed-precipitation events fall under the ROS category. When ROS and SOS events are described for the specific locations in Fig. 1, statistics are based on the events recorded for the single MERRA-2 grid cell containing each location.

d. *ROS links to storms*

To differentiate the synoptic characteristics of ROS events from SOS events, synoptic-scale cyclones were detected and tracked using the algorithm introduced by Crawford and Serreze (2016). After reprojecting the data to a 100 km polar equal-area grid (EASE-Grid 2.0) and masking grid cells with an elevation over 1500 m, cyclones are detected as local minima in SLP that have an average SLP gradient of at least 7.5 hPa over a 1000 km radius. "Local minimum" means that the SLP in a grid cell identified as a cyclone center is lower than its 24 nearest neighbors, and no more than 9 of those

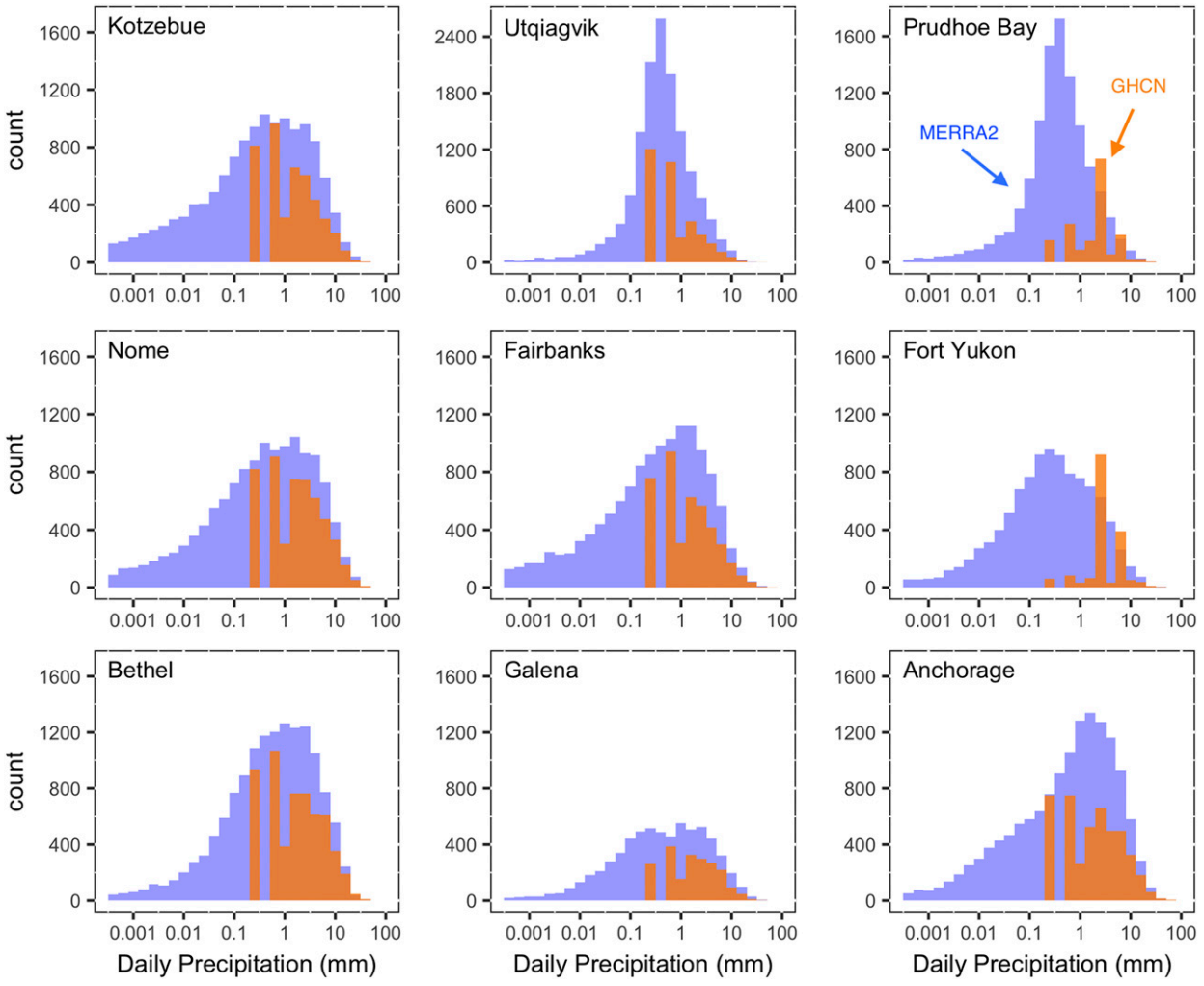

FIG. 2. Comparison of daily precipitation totals for nine selected locations in Alaska. The orange histograms are the distributions of daily precipitation totals measured at surface weather stations, and the blue histograms are the distribution of daily precipitation totals from corresponding MERRA-2 grid cells. The gap in the orange histogram occurs because the x axis is a log scale and precision for the weather stations is never finer than hundredths of an inch. Note that the precision of the Fort Yukon precipitation measurements is hundredths of an inch 1984–90 and tenths of an inch 1993–2018. Similarly, Prudhoe Bay records are precise to hundredths of an inch 1986–99 and tenths of an inch 2003–18. All other stations have data from 1980 to 2018 with precision of hundredths of an inch. The y axis is the same scale for all graphs except Utqiaġvik, which has a much narrower distribution than the other locations.

neighbors can be masked for elevation. Cyclone area is defined by the outermost closed isobar around a storm system. Multicenter cyclones are identified if 1) combining two centers into one system more than doubles the cyclone area and 2) those centers are no more than 1200 km apart. The lowest pressure center is considered the primary storm center. Cyclone identification is identical to Crawford and Serreze (2016), with two adjustments: 1) The number of neighbors used here is higher, and 2) The distance threshold between multicenter cyclones is increased. These modifications are necessary because the SLP fields of MERRA-2 are noisier than those of MERRA and yield more weak pressure minima. The modified parameters bring MERRA-2 cyclone statistics into better alignment with the results from MERRA and ERA-I reported in Crawford and Serreze (2016, 2017) (Tables S1 and S2).

Storm tracking was identical to Crawford and Serreze (2016). The movement of a storm between any time t_n and 3 h later at t_{n+3} is predicted based on past propagation. The closest cyclone center in t_{n+3} to the predicted location that results in a realistic propagation speed (less than 150 km h^{-1}) is adopted as a continuation of the track. Finally, tracks for cyclone centers that are part of the same multicenter cyclone are combined so that each storm system has a single track.

TABLE 2. Number of ROS and SOS events used in statistical comparisons. The months for which ROSF events have been observed are indicated; only ROS and SOS events in these months are included in the statistical analysis. Also indicated are the number and percentage of ROS and SOS events that were successfully linked to a storm track.

		All Events		Linked to a Storm Track			
Location	Months	ROS	SOS	ROS	%	SOS	%
Bethel	Oct–Mar	239	392	186	78%	345	88%
Anchorage	Oct–Feb	277	369	220	79%	327	89%
Galena	Oct–Feb	95	407	76	80%	286	70%
Nome	Oct–Feb	144	414	118	82%	341	82%
Fairbanks	Oct–Feb	57	255	51	89%	221	87%
Fort Yukon	Sep–Dec, Feb, Apr	55	224	49	89%	199	89%
Kotzebue	Oct–Dec, Feb	58	289	47	81%	222	77%
Utqiaġvik	Sep–Oct	37	54	27	73%	49	91%
Prudhoe Bay	Sep–Oct	32	56	24	75%	46	82%

Similar to past studies (e.g., Finnis et al. 2007; Stroeve et al. 2011; Crawford and Serreze 2017), precipitation events were linked to storms in two ways. The most straightforward relation is made when the location of a precipitation event lies within a cyclone system's area. Since SLP-based area does not neatly align with precipitation regions, a precipitation event is also linked to a storm if it lies within 1200 km of the storm's primary center. If multiple storms lie within 1200 km, the closest storm to the given location is chosen. Depending on the site, between 70% and 91% of events could be matched to a synoptic-scale cyclone track (Table 2). Results do not substantially change if longer-lived storms are preferentially linked to precipitation events (Table S3).

e. *Statistical comparisons of ROS events*

For nine grid cells in Alaska with suitably long station records for validation (see Fig. 1), composite maps of SLP, GPH at 500 hPa, precipitable water, and 2-m air temperature during ROS events in the period 1980–2018 were compared to composites of SOS events at the same location. Although ROS events were identified for all months at each location, composite analysis was conducted only for months with at least one ROSF event. This focuses analysis more specifically on ROS events likely to impact foraging, and it mitigates the possibility of detecting seasonal differences instead of storm-type differences. Note, though, that the number of valid months for comparison differs by location (Table 2). Because some of the sample populations are not normally distributed, the Mann–Whitney U statistic was used to assess the significance of observed differences.

In addition to composites, the spatial distribution of storm tracks associated with ROS events versus SOS events was compared. The number of ROS and SOS events is unequal (e.g., 27 vs 49 at Utqiaġvik, respectively), so a relative track density (the percentage of ROS-producing or SOS-producing tracks that pass within 250 km of each gridcell center) was used.

Since these fields have 1) high spatial autocorrelation and 2) strongly right-skewed distributions, a Monte Carlo simulation was used to assess whether the differences in relative track densities associated with a given location are significant. To avoid undue influence by outliers, only grid cells with a relative track density of 5% for all precipitation-on-snow-associated storms were considered. For each iteration of the simulation, the total number of precipitation-on-snow-associated storm tracks was randomly divided into two subpopulations whose sizes were based on the observations. (For example, Utqiaġvik has 27 ROS events and 49 SOS events, so for its Monte Carlo simulation, the population of 76 storm tracks was always divided into random groups numbering 27 and 49 observations each.) Next, the relative track density for each grid cell in the study area was calculated for each population. Finally, the chi-square distance ($\chi_{a,b}$) between the two populations was calculated, where a_i and b_i represent the relative storm track densities at location i for each population of tracks, and μ_i is the average relative storm track density at that location [Greenacre and Primicerio 2013; Eq. (1)]:

$$\chi_{a,b} = \sqrt{\sum \left[\frac{1}{\mu_i} (a_i - b_i)^2 \right]}. \quad (1)$$

One thousand iterations of this process were compared to the observed chi-square distance. If the observed chi-square distance exceeded the 95th percentile, then the observed populations of storm tracks were considered significantly distinct from one another.

Each storm track in the database has a genesis latitude and longitude, a track length, and a maximum intensity. The medians for these characteristics were compared between ROS- and SOS-producing storms at each location

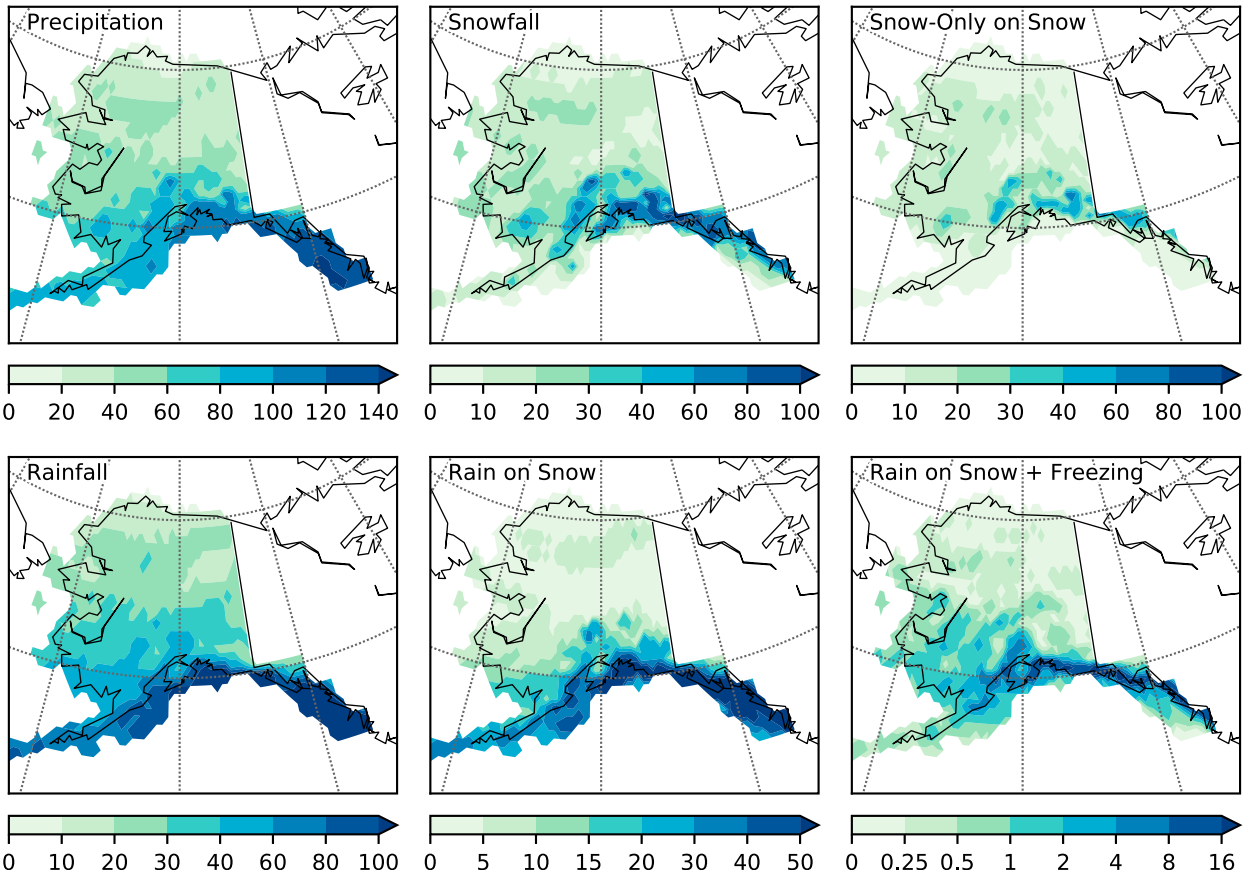

FIG. 3. Average annual count of precipitation events, snowfall events, SOS events involving no rain, rainfall events (including mixed precipitation), ROS events, and ROS events for which 95% of the following 720 h (30 days) have a subfreezing skin temperature. All data averaged from MERRA-2 over 1980–2018.

using the Mann-Whitney U test. Intensity was measured in three common ways: central pressure (p_{center}), depth (p_{edge}–p_{center}, where p_{edge} is the pressure of the last closed isobar), and the Laplacian of central pressure ($\nabla^2 p$).

3. Results and discussion

a. Spatial and seasonal distribution of ROS events

As stated above, ROS requires two elements: 1) a preexisting snowpack, and 2) precipitation in the form of rain. Alaska has a latitudinal precipitation gradient, with more precipitation events each year along the southern coast, fewer in the interior, and the fewest along the North Slope (Fig. 3). The mountainous southeast receives more precipitation events than the southwest, but north of the Alaska Range precipitation events are more common in the coastal west than the interior east. These general patterns apply to all subsets of precipitation, although the latitudinal gradient is especially prominent for rainfall and ROS events and slightly muted for ROSF events (for which 95% of the subsequent 720 h (30 days) have a subfreezing skin temperature). This occurs because a lower percentage of ROS events in the south are followed by prolonged freezing than in the interior (around 20% and 30%, respectively).

These spatial patterns, with the highest numbers of ROS events in the southeast, moderate values in the southwest, and sparingly few along the North Slope, is consistent with several past studies using reanalysis output (e.g., Putkonen and Roe 2003; Rennert et al. 2009; Cohen et al. 2015; Bieniek et al. 2018). Our counts are generally lower than those reported by Bieniek et al. (2018), likely because we limited classification of precipitation events to those with 2.54 mm per event rather than 0.254 mm day^{-1}. Our counts are better aligned with those of Rennert et al. (2009), who used a similar limit of 3 mm day^{-1}. Pan et al. (2018) identified a higher number of events in southwest Alaska than along the Gulf of Alaska, but this could be because their satellite-based approach can detect melt events unrelated to precipitation.

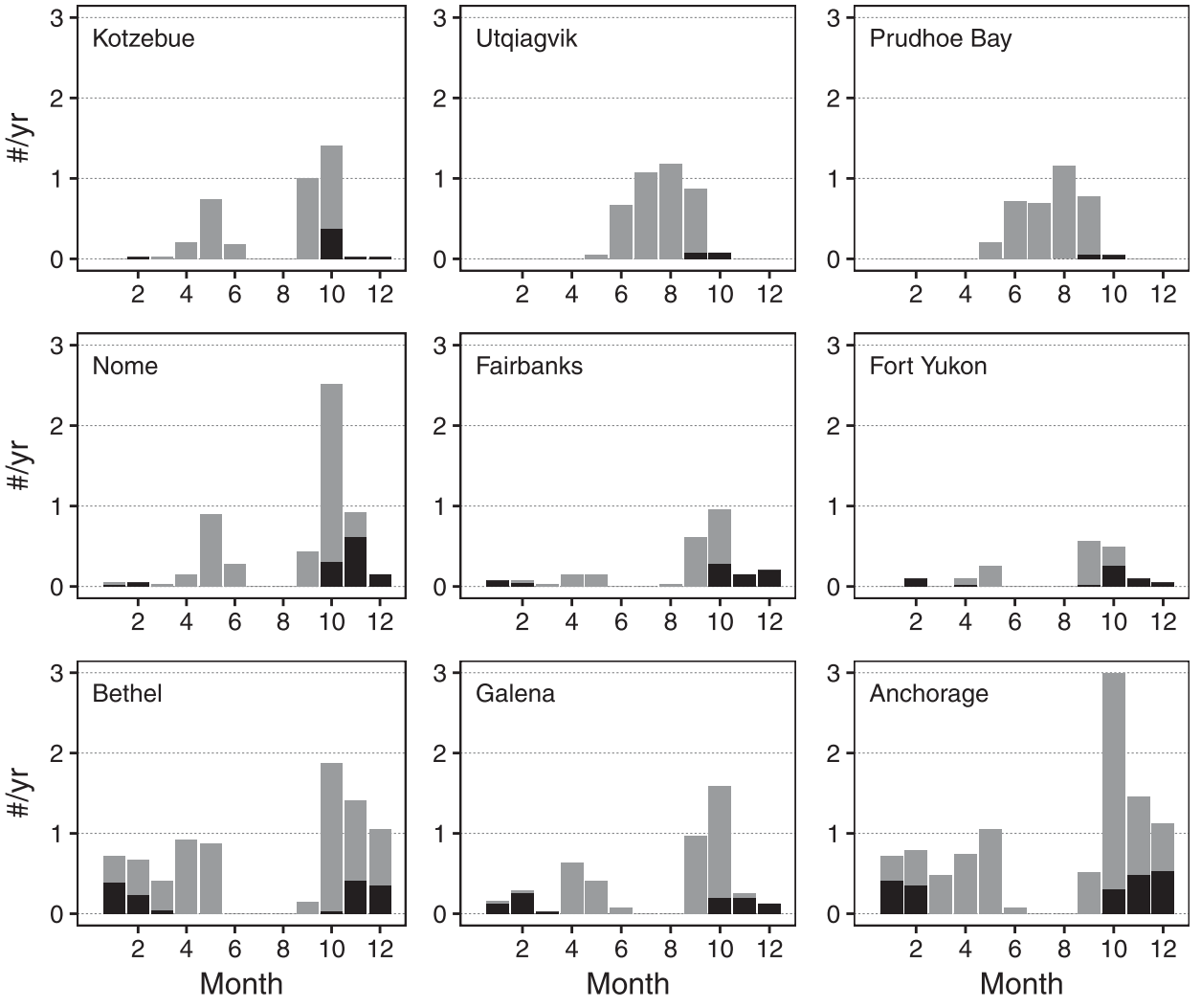

FIG. 4. Annual distribution of ROS events by month at nine locations in Alaska based on MERRA-2 ROS detection for the period 1980–2018. The black portion of each column indicates ROS events for which 95% of the following 720 h (30 days) have a subfreezing skin temperature. Similar plots including SOS events can be found in Fig. S2.

To focus more closely on seasonal patterns, the average number of ROS and ROSF events from 1980 to 2018 at the nine selected Alaskan sites (see Fig. 1) was determined for each month (Fig. 4 and Fig. S2). Kotzebue and Nome, both on the west coast, experience ROS events primarily in fall (SON) and spring (AMJ). However, Kotzebue, which is north of the Seward Peninsula and Bering Sea, experiences more ROS events than Nome in September, whereas Nome is more likely than Kotzebue to experience ROS in November. ROSF only occurs from October through February at each site.

Bethel, in the southwest, and Anchorage, on Cook Inlet along the Gulf of Alaska, have more even distributions of ROS events from October through May. These locations are more likely than Nome or Kotzebue to experience ROSF in December and January because they have warmer climates. Altogether, ROSF occurs on average about 1.5 and 2.1 times each winter in Bethel and Anchorage, respectively. Although farther north and more interior, Galena's seasonal distribution of ROS and ROSF is similar to Bethel's. The biggest differences are that Galena experiences more ROS events than Bethel in September but fewer in November and December.

The two interior sites, Fairbanks and Fort Yukon, are comparable to the southern and western sites in terms of when ROS and ROSF occur, but they differ in two ways: 1) they see no more than one ROS event per year in any month, and 2) a higher percentage of their ROS events are followed by prolonged freezing.

The two sites on the Beaufort Sea coast, Utqiaġvik, and Prudhoe Bay, are distinct because the vast majority

TABLE 3. Difference of median cyclone characteristics for ROS- and SOS-producing storms during months of interest for nine locations in Alaska. Bold text indicates significant values at $p < 0.05$; p values are calculated using the Mann–Whitney U statistic.

	Bethel	Anchorage	Galena	Fairbanks	Fort Yukon	Nome	Kotzebue	Utqiaġvik	Prudhoe Bay
Min pressure (hPa)	**4.89**	0.27	0.96	0.07	4.39	0.82	3.45	3.50	3.25
Max depth (hPa)	−2	2	2	0	−2	3	3	−8	−8
Max Laplacian [hPa (100 km^2)$^{-1}$]	−0.46	0.86	0.28	0.98	6.28	0.38	6.76	−0.86	−1.12
Track length (km)	−183	**1048**	**852**	490	604	**925**	**654**	266	−1205
Genesis latitude (°N)	1.71	**−3.63**	−2.32	−4.36	6.52	0.15	−2.84	5.31	4.83
Genesis longitude (°E)	−0.11	**−16.58**	**−14.00**	0.63	−5.99	**−13.52**	**−12.46**	−1.22	10.06

of ROS events are in the warmer months instead of the cooler or coldest months. This results in part because winter months are typically too cold for rain; however, summer is also the ''wet'' season along the North Slope. At both locations, the only two months with ROS events followed by prolonged freezing are September and October. One of the six ROSF events detected at Utqiaġvik is the 2–3 October 2003 event described by Brown (2005).

These results have implications for any comparison of synoptic conditions associated with ROS events. First, if storms producing ROS are compared to all storms impacting a location, any observed differences may simply result from the fact that ROS events only occur in certain months. For example, Nome tends to experience its strongest storms in October and November (Mason et al. 1996), and the synoptic patterns most associated with precipitation in the Yukon basin differ between summer and winter (Cassano and Cassano 2010). Comparing ROS-producing storms to SOS-producing storms in months when both can occur alleviates the problem of seasonality as a confounding variable. Second, ROS events occur in different months depending on the location, implying that a variable observation period must be used. Some studies have compared anomalies in atmospheric variables associated with ROS events to climatological means for an entire season [e.g., October–March (Rennert et al. 2009) or September–November and December–February (Cohen et al. 2015)]. These seasons work for some locations, but they would be problematic at Utqiaġvik, for example, where ROS events occur May–October. Third, the most dangerous ROS events for ungulates are ROSF events, which have an even more restricted seasonality (Fig. 4). For this reason, the synoptic conditions related to ROS-producing and SOS-producing storms are only compared in this study for months in which there are observed ROSF events (Table 2). All ROS events in those months are considered, however. While the characteristics of individual cyclones influence whether snow or rain falls during a precipitation event, they are not expected to dictate whether the temperature during the following 720 h is consistently subfreezing.

b. *Cyclone tracks related to ROS vs SOS*

One straightforward comparison between ROS- and SOS-producing cyclones is with respect to characteristics such as storm intensity, track length, and genesis location (Table 3). Results show no consistently significant difference between ROS- and SOS-producing storms at any of the nine sites for the three common storm intensity measures (central pressure, the Laplacian of central pressure, or cyclone depth). However, for four of the nine sites, ROS-producing storms tend to form significantly farther west and have significantly longer average track lengths than SOS-producing storms. For no location are ROS-producing storm tracks significantly shorter or generated farther east. In other words, ROS-producing storms cannot be differentiated from SOS-producing storms based on their intensity, but they may be distinguishable by where they form and track.

To further investigate whether ROS-producing and SOS-producing storms can be differentiated, we compared spatial patterns of relative track density for storms that produced ROS at a particular location (i.e., grid cell) to those that produced SOS at the same location. Bethel is introduced as an example first; the other locations are then added. Bethel experiences ROSF events from October–March, so the first step was selecting all October–March storms (1980–2018) that produced ROS at this location. Next, a map of relative track density was created (Fig. 5, top left) by calculating the percentage of the selected ROS-producing tracks that passed within 250 km of each gridcell center. This map of storm-track density includes the entirety of each storm track, allowing us to examine not only where low-pressure centers are located during ROS events, but also where the cyclones come from and where they travel to. By normalizing storm-track density, the dataset becomes more directly comparable to other populations of storm tracks that may include more or fewer storms.

ROS-producing storms affecting Bethel are most frequently part of the North Pacific storm track and

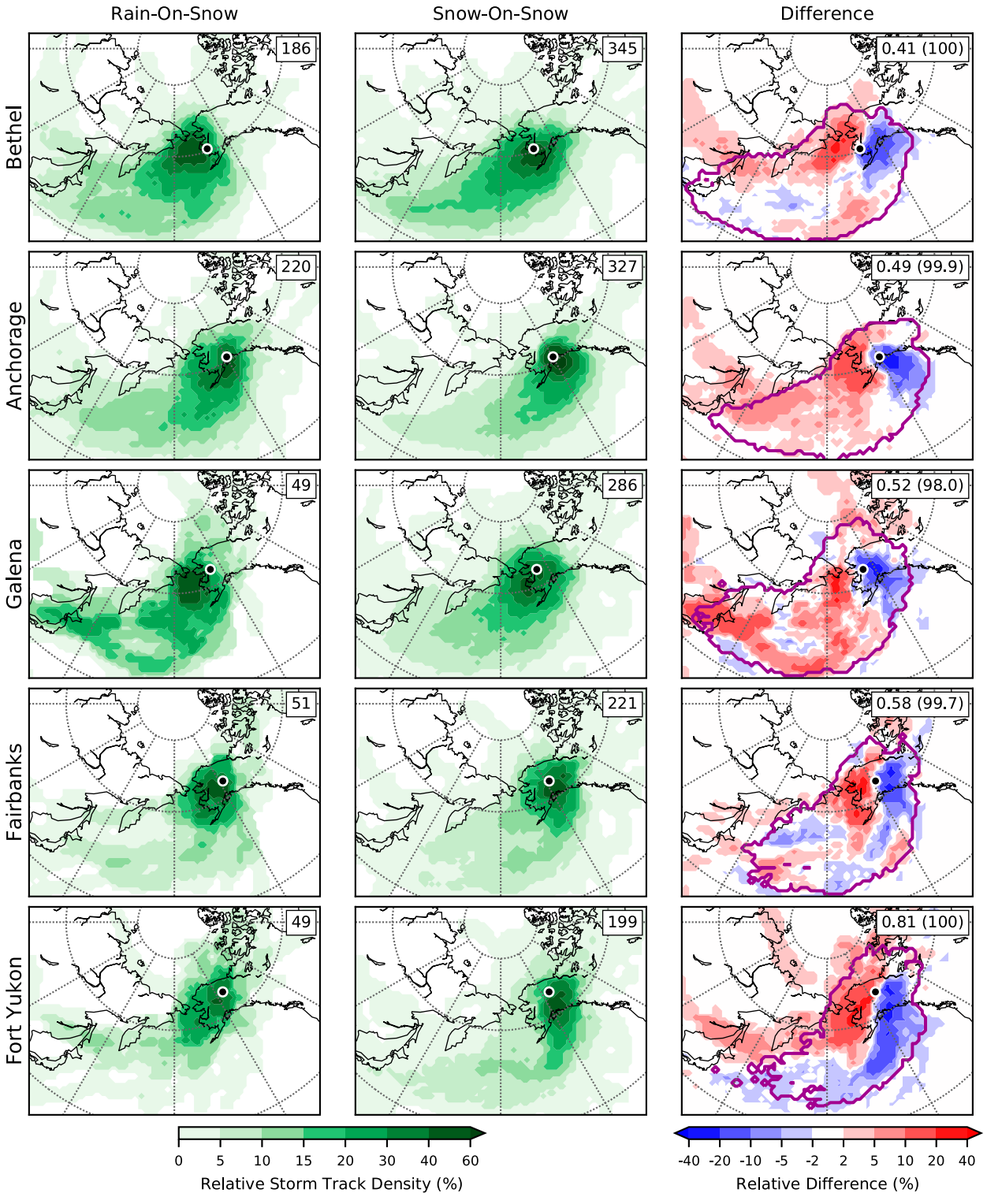

FIG. 5. Relative storm-track density for storms impacting five locations (black dots) during 1980–2018 that produce either (left) rain-on-snow or (middle) snow-on-snow events that involve no rain, and (right) their difference (% ROS − % SOS). A relative average (percentage of ROS-producing or SOS-producing tracks that pass within 250 km of each grid cell) is used to make the two populations of storm tracks more comparable. Numbers in the top right indicate population size for the first two columns. For the third column, they indicate the chi-square difference between these two populations of storm tracks and the percentile of that statistic when compared to a 1000-member Monte Carlo simulation using the spatial domain outlined in dark magenta. (To avoid undue influence by outliers, only grid cells with a relative track density of 5% for all linked storms were used to calculate chi-square distances.)

migrate into the Bering Sea west of Bethel. This may not seem notable since most storms affecting southwest Alaska come from the North Pacific storm track (Wernli and Schwierz 2006), but the northern Bering Sea is only a secondary cyclolysis area; most North Pacific storms migrate into the Gulf of Alaska (Mesquita et al. 2010). Furthermore, storms that produce SOS events at Bethel (Fig. 5, top center) tend to take a more southerly path. They sometimes stay in the Bering Sea, but more often they migrate past Bethel and into the Gulf of Alaska. Such paths tend to put Bethel in the cold sector of the cyclone, hence being less likely to produce rain over Bethel. This difference becomes even more apparent when subtracting the SOS track densities from the ROS track densities (Fig. 5, top right). The red areas in this figure show where ROS-producing storms are relatively more likely to track; the blue areas show where SOS-producing storms are relatively more likely.

To assess whether the difference in these spatial patterns is significant, we used the 1000-member Monte Carlo simulation described in section 2e and a chi-square distance measure of dissimilarity. The larger the chi-square distance, the more distinct the two patterns; however, the more relevant number in the upper right of the difference plots in Fig. 5 is the percentile. A value of 100 means that none of the patterns in the Monte Carlo simulation yielded a higher chi-square distance than the observed pattern of ROS-producing tracks versus SOS-producing tracks. This confirms that the spatial pattern of storms producing ROS at Bethel is statistically distinct from the pattern of storms producing SOS.

Turning to the remaining eight regions, the situations for Galena, Anchorage, Fort Yukon, and Fairbanks are similar to what was found for Bethel (Fig. 5), with a strong west-east distinction between ROS- and SOS-producing storms. ROS-producing tracks are located preferentially to the northwest, especially over the northern Bering Sea, and SOS-producing tracks are relatively more likely in the Gulf of Alaska and the interior. Regional differences are also apparent. For example, Fairbanks and Fort Yukon experience a greater percentage of storms of both types striking into the interior. Also, whereas SOS-producing storms at Bethel and Galena have more diverse tracks than ROS-producing storms, the opposite is true for Anchorage. Storms producing ROS at Anchorage can track either into the Gulf of Alaska or the northern Bering Sea, but SOS-producing tracks are nearly always restricted to the Gulf of Alaska (Fig. 5, second row). Despite some regional differences, one general result is similar for all sites in Fig. 5: SOS-producing storms are more likely to track into the Gulf of Alaska.

Nome is interesting because neither ROS-producing nor SOS-producing storms typically track into the Gulf of Alaska (Fig. 6, top row). The distinction here is more prominently north–south, with SOS-producing storms more likely to take a more southerly route through the North Pacific. Fort Yukon also shows this pattern (Fig. 5, bottom row). Additionally, storms producing ROS at Nome are relatively more likely to originate in the extreme western Pacific (e.g., between Hokkaido and Kamchatka) than storms producing SOS. This is also true for ROS-producing storms at several other sites (Bethel, Anchorage, Galena, and Kotzebue), including all sites for which the average genesis longitude for ROS-producing storms was farther west than for SOS-producing storms (Table 3).

Results from the Monte Carlo simulations for all six of the locations discussed above show that observed patterns are above the 95th percentile, indicating a significant distinction between ROS- and SOS-producing storm tracks. However, the percentiles for Kotzebue, Utqiaġvik, and Prudhoe Bay are not significant (Fig. 6). Maps for the two North Slope sites do suggest that ROS-producing storms may have a greater tendency to track through Bering Strait, but these results are based on very few precipitation events (Table 2). This is why results are insignificant; it could be that a few ROS-producing storms by chance took a similar route rather than a systematic difference. All three of these sites are more strongly affected by storms from the Arctic storm track than the rest of Alaska, especially Prudhoe Bay and Utqiaġvik (Crawford and Serreze 2016), and the production of ROS or SOS in Alaska by these Arctic storms may be less dependent on storm path than for Pacific storms. Moreover, any Pacific storm in September or October occurs under a weaker midlatitude waveguide than do Pacific storms in winter, which may lead to more variability in storm tracks. Regardless of the reason, it is only for locations strongly influenced by the North Pacific storm track that we can be confident in a clear distinction between the tracks of ROS- and SOS-producing cyclones.

c. Large-scale atmospheric setting for ROS vs SOS

To further illustrate how differences in storm tracks dictate whether ROS or SOS occurs, we compared composites and detrended composite anomalies of SLP, GPH at 500 hPa, 2-m air temperature, and precipitable water for ROS events to those for SOS events. Although detrended composite anomalies are the focus of this section, the raw composite fields for the hour during which ROS or SOS events begin is shown in Figs. S3 and S4. The ROS composite plot for Bethel (top left of Fig. S3) is comparable to Fig. 5c from Rennert et al. (2009); when

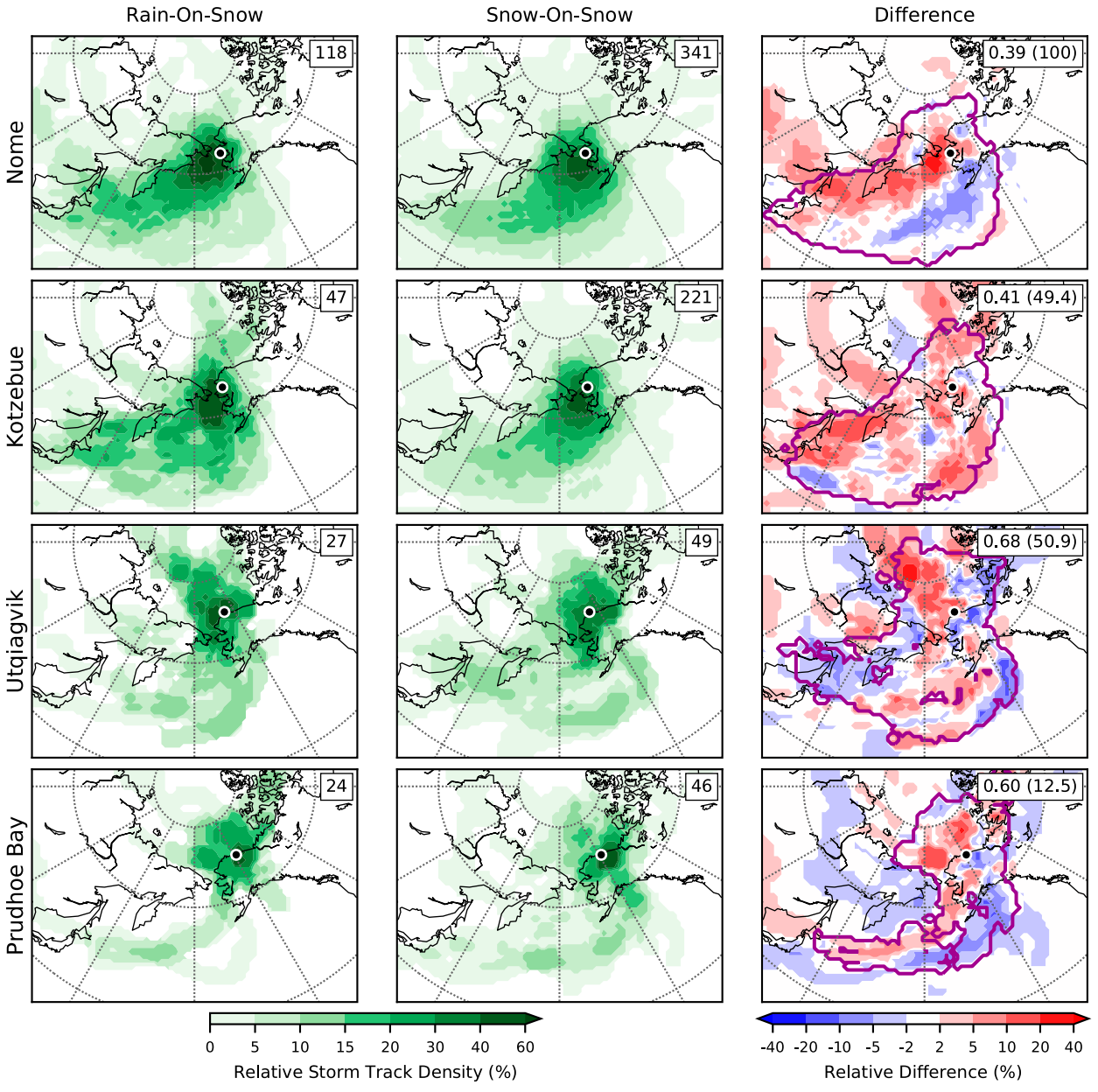

FIG. 6. As in Fig. 5, but for four additional locations in Alaska.

ROS occurs in southwest Alaska, there is typically a trough to the west and a ridge to the east and southeast at the 500 hPa level. This basic pattern also holds for ROS events at most other sites: ROS events involve low pressure centers located on average slightly downstream of the trough axis, which is typical of maturing cyclones. Utqiaġvik and Prudhoe Bay are the exceptions, as they lack a well-defined low pressure location for ROS events (Fig. S4). However, these synoptic plots for ROS events alone are insufficient to show a distinct ROS signature because an upper-level trough with low sea level pressure to the west and a ridge to the east also describes many other precipitation events at these sites, including SOS events (center column of Figs. S3 and S4).

Additionally, comparisons of ROS and SOS events in this dataset are better suited for detrended composite anomalies. Even after limiting analysis to months for which ROSF events occur, ROS is more common than SOS in some months and less common than SOS in others (Fig. S2). Using composite anomalies (for which anomalies are calculated with respect to the monthly climatology) removes any seasonal effect. Additionally,

long-term atmospheric trends are present in the data. ROS events are becoming more common over much of Alaska (e.g., Nome experienced 2.2, 3.6, 4.4, and 4.7 ROS events per year for 1980–89, 1990–99, 2000–09, and 2010–18, respectively.) At the same time, temperature and precipitable water, but also SLP and GPH, have experienced significant trends in this region over the past 40 years (Hartmann et al. 2013). Therefore, composites were compiled after removing the linear trend from 1980 to 2018 for each MERRA-2 anomaly variable from all grid cells. Therefore, the remainder of this study will focus on detrended composite anomalies of atmospheric variables.

When considering composite differences of detrended anomalies in SLP and GPH (right-hand column of Fig. 7), Bethel and Anchorage exhibit the strongest distinctions between ROS and SOS events. For both sites, the anomalous ridge in GPH contours to the east is much stronger for ROS than SOS events, and SLP anomalies are significantly higher ($p < 0.05$). Both also exhibit significantly stronger negative SLP anomalies located to the west for ROS than for SOS. Fairbanks, Fort Yukon, and Galena show weaker but similar patterns, especially the stronger ridging to the east for ROS events (Fig. 7). This is similar to findings by Bieniek and Walsh (2017) and Bieniek et al. (2018), who reported that for several sites in Alaska, anomalously high pressure to the southeast was the most distinct SLP pattern for heavy precipitation and heavy ROS events, respectively. Stationary upper-tropospheric ridges (associated with surface high pressure centers or ''blocking highs'') can slow or deflect poleward the trajectory of synoptic-scale cyclones (Mesquita et al. 2009; Wang et al. 2014). Stronger surface anticyclones also enhance the pressure gradient on the east side of the storm, increasing poleward flow and the advection of warmer, moister air (Rex 1950; Massom et al. 2004; Liu et al. 2016) that is more likely to produce rain over the snowpack.

October 1992 provides a good example, when a blocking event south of the Aleutian Islands deflected a storm northward through the Bering Strait (Mesquita et al. 2009; Pezza et al. 2010). This storm intensified rapidly and caused $6 million of damage in Nome largely from storm surge (Blier et al. 1997), but it also produced ROS throughout the west coast, southwest, and interior regions of Alaska. A similar mechanism may be responsible for many storms producing ROS in Alaska. When a cyclone tracking along the North Pacific storm track is confronted with a blocking upper-tropospheric ridge, it is diverted to the north, placing it in a prime position to induce southerly flow, which brings with it warmer and moister air that is more likely to produce rain than other cold-season cyclones.

The same five sites for which a clear distinction can be made between ROS and SOS composite detrended anomalies (Bethel, Galena, Anchorage, Fairbanks, and Fort Yukon) are also the sites that show significant east to west differences in the relative track densities of ROS-producing versus SOS-producing storms (Fig. 5). Also consistent with results from section 3b, the three locations lacking clear distinction between ROS and SOS storm tracks (Fig. 6) have different patterns in composites (Fig. 8). Utqiaġvik and Prudhoe Bay both have similar detrended anomalies to Bethel, with more positive anomalies in SLP and GPH to the east during ROS events (right-hand column) than during SOS events (center column); however, this is more because low SLP is not as low during ROS, not because high SLP is higher (Fig. S4). Kotzebue, by contrast, shows a pattern nearly opposite of most other sites. High pressure and GPH anomalies dominate to the southeast of Kotzebue during both ROS and SOS, but the anomalies are significantly stronger during SOS events.

The only site for which results are inconsistent is Nome. Although the tracks for storms producing ROS at Nome were distinct from those producing SOS (Fig. 6, top row), the distinction was mostly that ROS-producing storms were more likely to have a more northerly track, not a more westerly track as with nearby Bethel or Galena. Nome also shows no difference in detrended anomalies of SLP or GPH between ROS and SOS events (Fig. 8, top row), although stronger distinctions appear if the raw SLP and GPH values are composited (Fig. S4). This likely reflects the difference in seasonality between ROS and SOS at Nome biasing results (Fig. S2). Therefore, results for Nome in Fig. 6 should be viewed with caution.

d. Temperature and precipitable water for ROS vs SOS

The stronger SLP and GPH anomalies at the start of ROS compared to SOS events at Bethel and Anchorage coincide with stronger positive anomalies in both 2-m air temperature and precipitable water (Fig. 9; raw composites in Figs. S5 and S6). This is consistent both with the northward displacement of tracks during ROS and the stronger pressure gradient produced by a stronger high pressure center during ROS. Fairbanks, Galena, and Fort Yukon also exhibit stronger positive anomalies in 2-m air temperature during ROS events, but more prominent for these sites is the different amount of precipitable water during ROS versus SOS. For all five of these sites in Fig. 9, the positive precipitable water anomalies during ROS extend from 45° to 70°N (Fig. S6) and are much stronger than during SOS events. Heavy precipitation events in Alaska have been previously

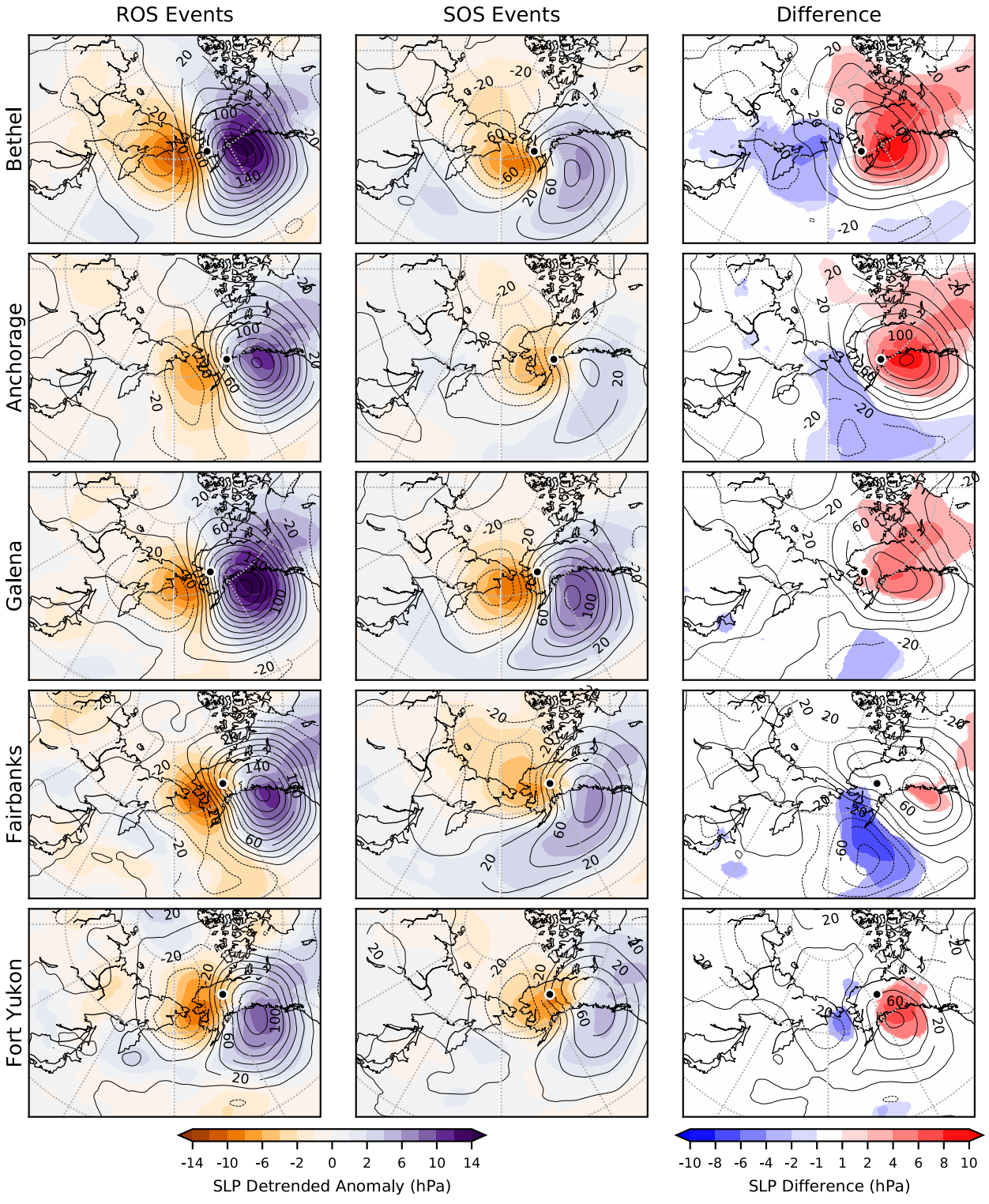

FIG. 7. Composites of detrended anomalies for synoptic conditions at the start of (left) ROS and (middle) SOS and (right) their difference (ROS − SOS) for five locations in Alaska (black dots) during the period 1980–2018. Filled contours are used for SLP and black contours are used for GPH at 500 hPa (20 m interval). Only significant SLP differences ($p < 0.05$) are shown in the difference plots.

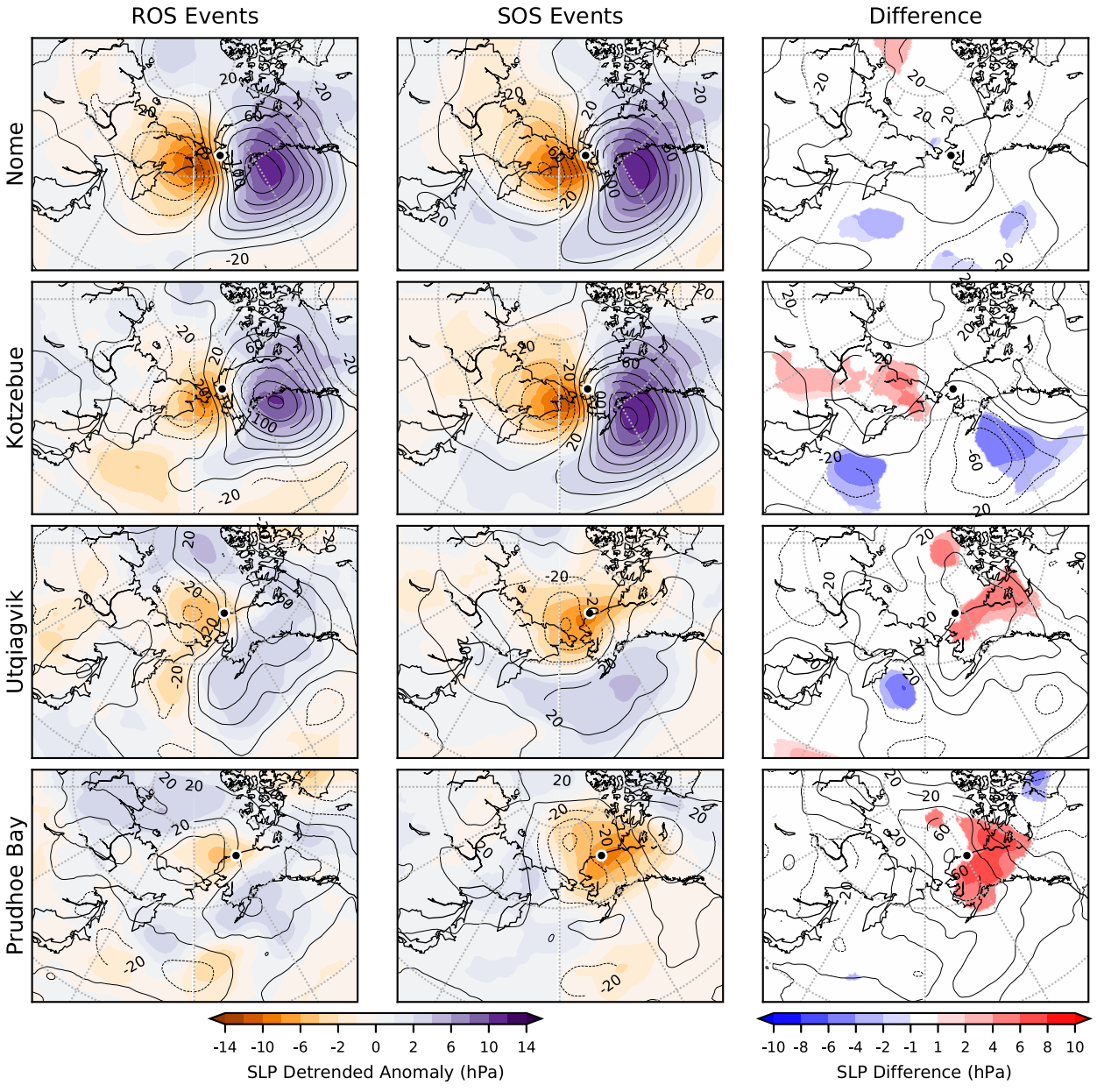

FIG. 8. As in Fig. 7, but for four additional Alaska locations.

linked to atmospheric rivers (Mundhenk et al. 2016; Bieniek et al. 2018). The composites of precipitable water anomalies presented here suggest that atmospheric rivers may be important for many ROS events along the Gulf of Alaska and in the interior, not only for the most extreme examples.

Consistent with section 3c, the four sites with less distinction between ROS and SOS for SLP and GPH also show little difference between ROS and SOS for 2-m air temperature and precipitable water (Fig. 10; raw composites in Figs. S7 and S8). Of the four sites, Kotzebue shows the biggest difference, with stronger precipitable water anomalies over Alaska during ROS than SOS. Very few differences are significant for Nome, Utqiaġvik, or Prudhoe Bay.

e. *Atmospheric conditions 72 hours prior to ROS vs SOS*

Results presented so far show that for the interior, southwest, and Gulf coast of Alaska, ROS events are distinct from SOS events whether looking at the spatial distributions of cyclone tracks that lead to the event type

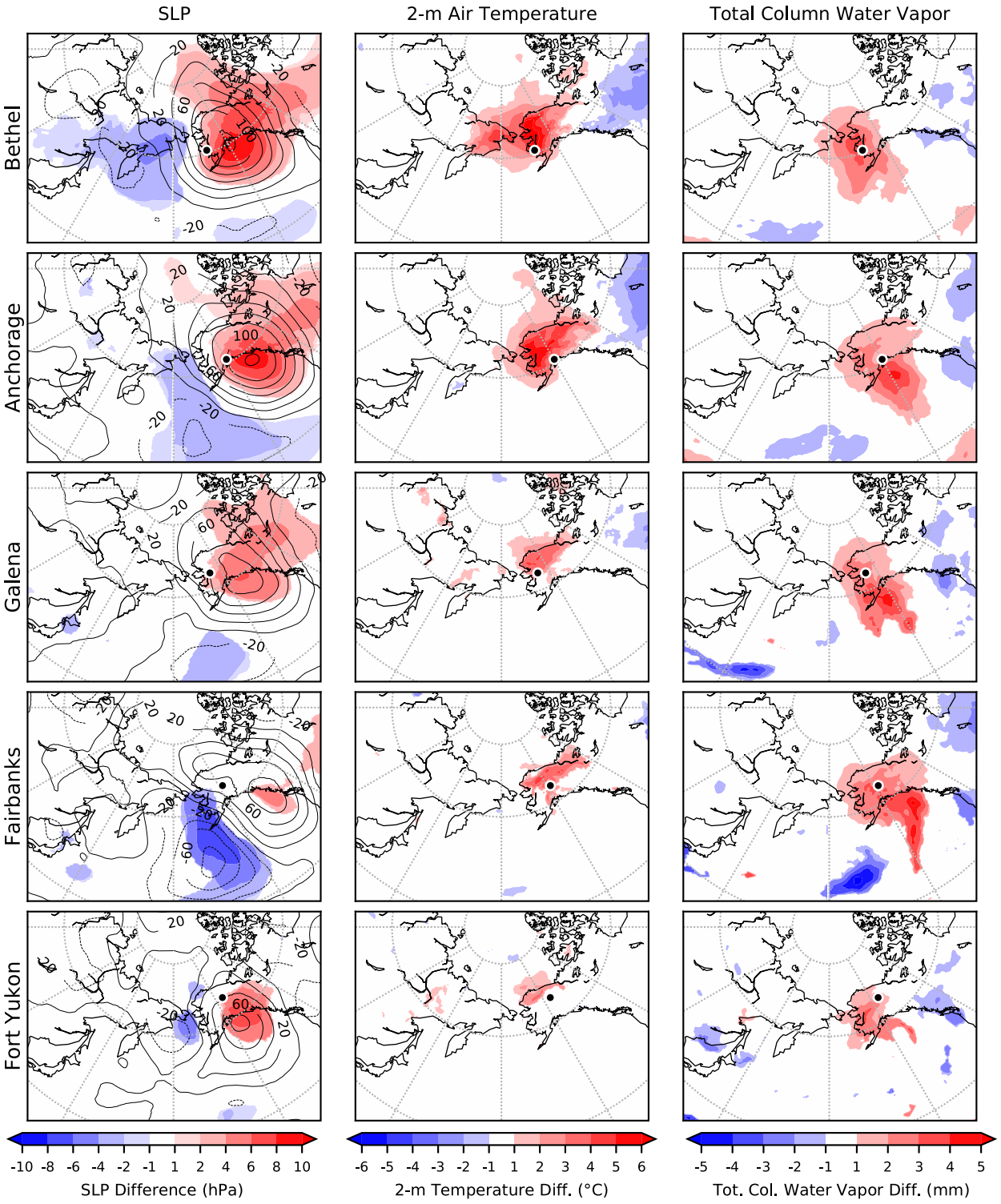

FIG. 9. Detrended composite anomaly differences at the start of (left) ROS and (middle) SOS and (right) their difference (ROS − SOS) for five Alaska locations (black dots) during the period 1980–2018. Variables included are (left) SLP (filled contours) and GPH at 500 hPa (contours with 20 m interval), (middle) 2-m air temperature, and (right) total column water vapor. Filled contours are only shown for significant differences ($p < 0.05$).

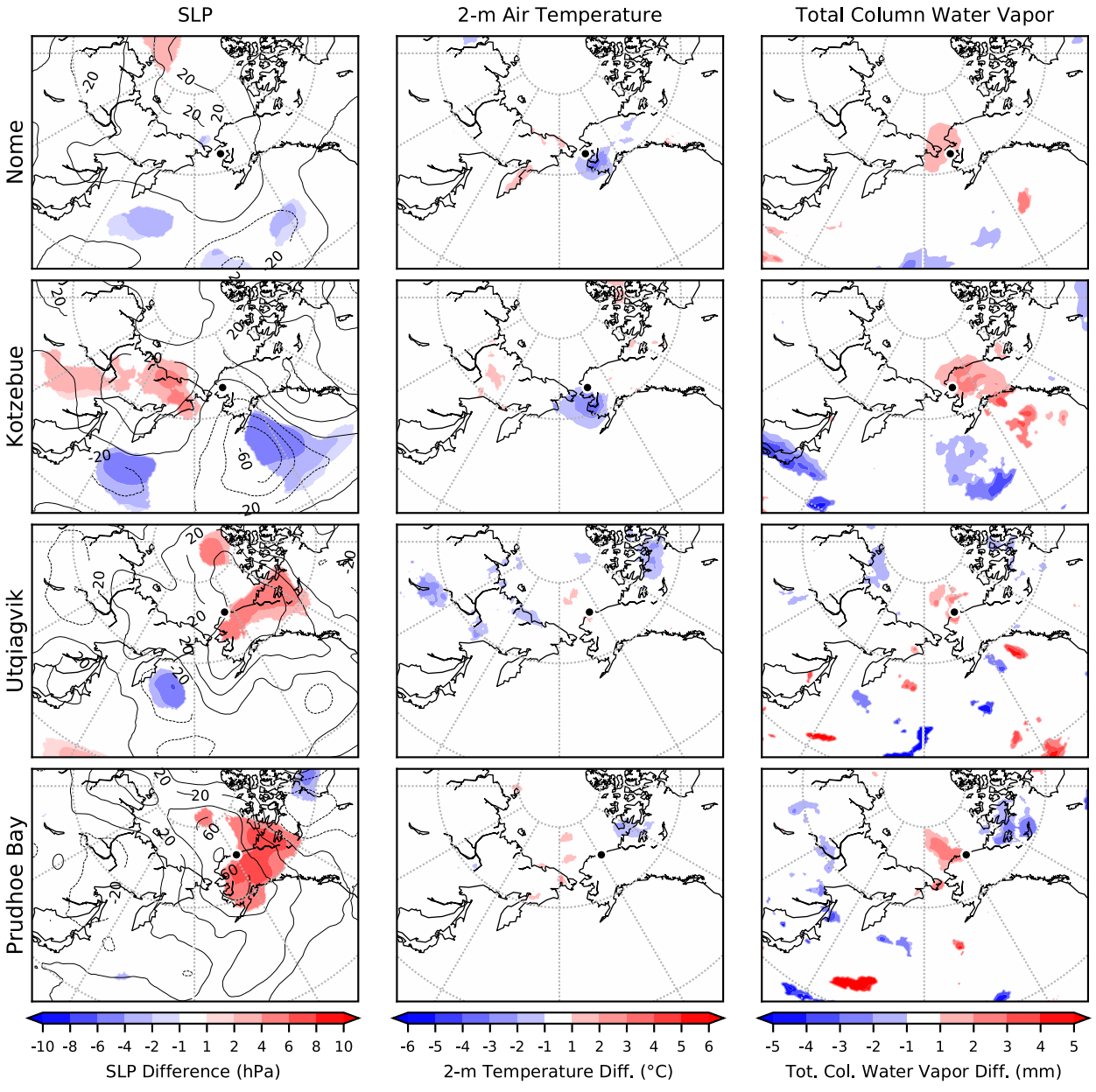

FIG. 10. As in Fig. 9, but for four additional Alaska locations.

or at the spatial patterns of SLP, GPH, temperature, and precipitable water at the initiation of each event type. However, in a predictive scheme, such distinctions are only useful if they can be made several days prior to the ROS or SOS event. Additionally, if the observed GPH and SLP patterns (section 3c) represent atmospheric blocking that cause cyclone deflection and therefore encourage ROS over SOS, the high SLP and GPH anomalies must precede the arrival of the cyclone. As a step toward addressing these issues, Figs. 11 and 12 show composite anomaly differences 72 h before ROS or SOS event initiation at each site. Other lag times (e.g., 60 and 120 h) were also examined and yielded consistent results (not shown). The raw composites for SLP and GPH, 2-m air temperature, and precipitable water are shown in Figs. S9-S10, S11-S12, and S13-S14, respectively.

For Bethel, Anchorage, and to a lesser degree Fairbanks, temperature and precipitable water anomalies are more positive 72 h before ROS than they are 72 h before SOS (Fig. 11), although less distinctly than at the time an event starts (Fig. 9). Strong positive anomalies in both GPH and SLP in the Gulf of Alaska for ROS compared to SOS are

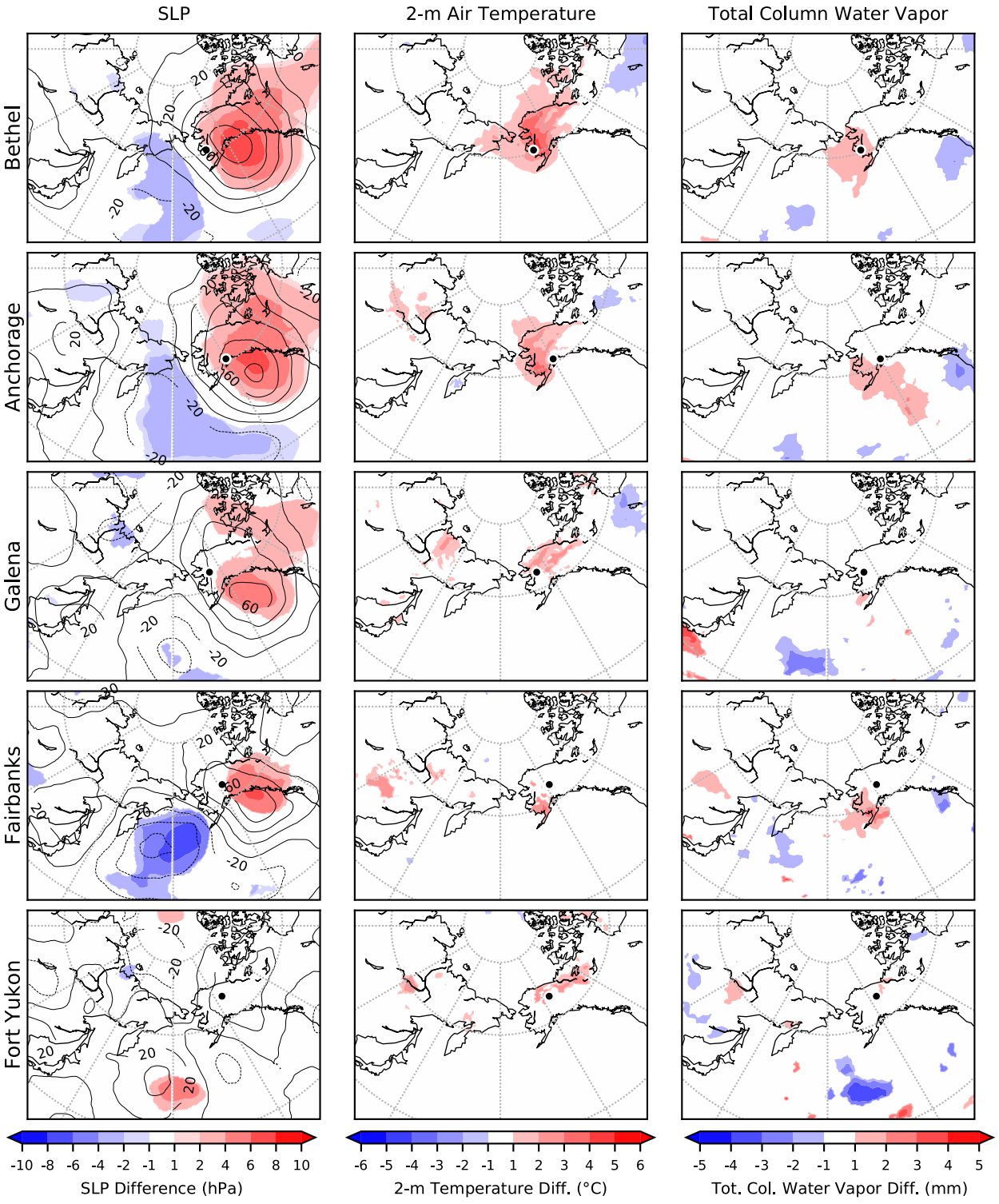

FIG. 11. Detrended anomaly composite differences (ROS − SOS), as in Fig. 9, only for 72 h prior to the start of ROS or SOS events.

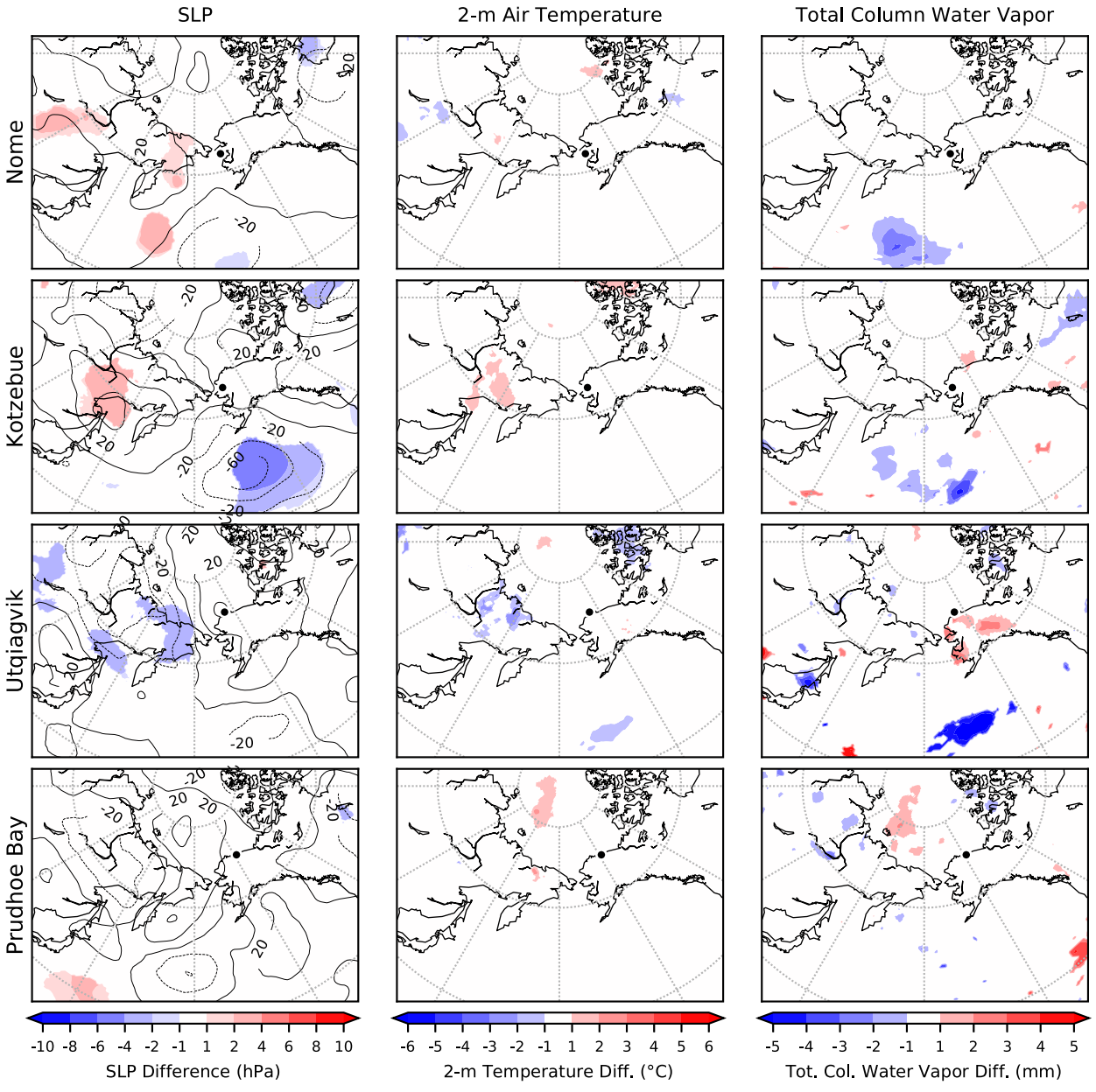

FIG. 12. As in Fig. 11, only for four additional Alaska locations.

still obvious for these three sites and for Galena, which indicates a persistent feature. This strengthens the idea that ROS often occurs at these locations because North Pacific cyclones are deflected northward by blocking upper-tropospheric ridges. Fort Yukon, however, which also showed distinct patterns at the time of SOS or ROS initiation, does not show persistence in the composite differences 72 h beforehand. Neither does Nome (Fig. 12). There is also no clear distinction between ROS and SOS events at Kotzebue, Utqiaġvik, or Prudhoe Bay, for which (as discussed previously) there were no significant differences in the spatial patterns of storm tracks. Hence, in general, sites farther south tend to show 1) more distinctions between ROS events and SOS events and 2) stronger influence by atmospheric blocking on ROS, which is detectable up to 72 h in advance.

4. Conclusions

Although ROS can occur throughout Alaska, there is substantial regional variation in the seasonality and

frequency of such events, as well as the tendency for ROS to lead to icing that inhibits ungulate foraging. ROS followed by prolonged freezing only occurs in September and October along the North Slope; it occurs as late as April in the interior; and south of the Brooks Range, it is most common from October to February. With this spatial diversity in mind, we examined whether the synoptic conditions leading to ROS were distinct from those leading to SOS during months in which ROS followed by prolonged freezing is possible.

Clear distinctions in synoptic conditions between ROS and SOS events were found only for the parts of Alaska that are strongly influenced by the North Pacific storm track. ROS-producing storms are not more intense than SOS-producing storms, but for six of the sites examined, ROS-producing storms are more likely to propagate northeastward into the Bering Sea and less likely to migrate eastward into the Gulf of Alaska compared to SOS-producing storms. This places ROS-producing tracks to the north and west of SOS-producing tracks on average, making southerly winds and warmer, moister, rain-producing air more common.

Additionally, ROS events at five of these sites (Anchorage, Bethel, Fairbanks, Fort Yukon, and Galena) are more frequently associated with a blocking upper-tropospheric ridge to the southeast than are SOS events. For four of these five sites, stronger positive anomalies in SLP and GPH associated with ROS compared to SOS were sufficiently distinct 72 h prior to the onset of events, indicating the potential value of high SLP as a statistical predictor for ROS events. This atmospheric blocking helps explain the different storm trajectories because they tend to deflect storm tracks. They also can increase the chances of rainfall because a steeper zonal pressure gradient enhances meridional flow. Future research could assess this linkage more rigorously with statistical or dynamical models and employ a more systematic detection and comparison of atmospheric blocking events.

Acknowledgments. The authors thank three anonymous reviewers for their constructive comments. The code used to generate these results from MERRA-2 and the GHCN can be found at https://github.com/alexcrawford0927/cyclonetracking and https://github.com/alexcrawford0927/rainonsnow. Support for this research comes from Grant ICER 1928230 from the National Science Foundation.

REFERENCES

Aanes, R., B.-E. Sæther, and N. A. Øritsland, 2000: Fluctuations of an introduced population of Svalbard reindeer: The effects of density dependence and climatic variation. *Ecography*, **23**, 437–443, https://doi.org/10.1111/j.1600-0587.2000.tb00300.x.

Bieniek, P. A., and J. E. Walsh, 2017: Atmospheric circulation patterns associated with monthly and daily temperature and precipitation extremes in Alaska. *Int. J. Climatol.*, **37**, 208–217, https://doi.org/10.1002/joc.4994.

——, U. S. Bhatt, J. E. Walsh, R. Lader, B. Griffith, J. K. Roach, and R. L. Thoman, 2018: Assessment of Alaska rain-on-snow events using dynamical downscaling. *J. Appl. Meteor. Climatol.*, **57**, 1847–1863, https://doi.org/10.1175/JAMC-D-17-0276.1.

Blier, W., S. Keefe, W. A. Shaffer, and S. C. Kim, 1997: Storm surges in the region of western Alaska. *Mon. Wea. Rev.*, **125**, 3094–3108, https://doi.org/10.1175/1520-0493(1997)125<3094:SSITRO>2.0.CO;2.

Boisvert, L. N., M. A. Webster, A. A. Petty, T. Markus, D. H. Bromwich, and R. I. Cullather, 2018: Intercomparison of precipitation estimates over the Arctic Ocean and its peripheral seas from reanalyses. *J. Climate*, **31**, 8441–8462, https://doi.org/10.1175/JCLI-D-18-0125.1.

Brown, C., Ed., 2005: Caribou management report of survey and inventory activities: 1 July 2002–30 June 2004. Alaska Department of Fish and Game, 292 pp.

Cassano, E. N., and J. J. Cassano, 2010: Synoptic forcing of precipitation in the Mackenzie and Yukon River basins. *Int. J. Climatol.*, **30**, 658–674, https://doi.org/10.1002/joc.1926.

Cohen, J., H. Ye, and J. Jones, 2015: Trends and variability in rain-on-snow events. *Geophys. Res. Lett.*, **42**, 7115–7122, https://doi.org/10.1002/2015GL065320.

Conway, H., and C. F. Raymond, 1993: Snow stability during rain. *J. Glaciol.*, **39**, 635–642, https://doi.org/10.1017/S0022143000016531.

——, and R. Benedict, 1994: Infiltration of water into snow. *Water Resour. Res.*, **30**, 641–649, https://doi.org/10.1029/93WR03247.

Crawford, A. D., and M. C. Serreze, 2016: Does the summer Arctic frontal zone influence Arctic Ocean cyclone activity? *J. Climate*, **29**, 4977–4993, https://doi.org/10.1175/JCLI-D-15-0755.1.

——, and ——, 2017: Projected changes in the Arctic frontal zone and summer Arctic cyclone activity in the CESM large ensemble. *J. Climate*, **30**, 9847–9869, https://doi.org/10.1175/JCLI-D-17-0296.1.

Dolant, C., A. Langlois, B. Montpetit, L. Brucker, A. Roy, and A. Royer, 2016: Development of a rain-on-snow detection algorithm using passive microwave radiometry. *Hydrol. Processes*, **30**, 3184–3196, https://doi.org/10.1002/hyp.10828.

Finnis, J., M. M. Holland, M. C. Serreze, and J. J. Cassano, 2007: Response of Northern Hemisphere extratropical cyclone activity and associated precipitation to climate change, as represented by the Community Climate System Model. *J. Geophys. Res.*, **112**, G04S42, https://doi.org/10.1029/2006JG000286.

Forbes, B. C., and Coauthors, 2016: Sea ice, rain-on-snow and tundra reindeer nomadism in Arctic Russia. *Biol. Lett.*, **12**, 20160466, https://doi.org/10.1098/rsbl.2016.0466.

Freudiger, D., I. Kohn, K. Stahl, and M. Weiler, 2014: Large-scale analysis of changing frequencies of rain-on-snow events with flood-generation potential. *Hydrol. Earth Syst. Sci.*, **18**, 2695–2709, https://doi.org/10.5194/hess-18-2695-2014.

Gelaro, R., and Coauthors, 2017: The Modern-Era Retrospective Analysis for Research and Applications, version 2 (MERRA-2). *J. Climate*, **30**, 5419–5454, https://doi.org/10.1175/JCLI-D-16-0758.1.

Greenacre, M., and R. Primicerio, 2013: *Multivariate Analysis of Ecological Data*. Fundación BBVA, 331 pp.

Hansen, B. B., R. Aanes, and B.-E. Sæther, 2010: Feeding-crater selection by high-Arctic reindeer facing ice-blocked pastures. *Can. J. Zool.*, **88**, 170–177, https://doi.org/10.1139/Z09-130.

——, ——, I. Herfindal, J. Kohler, and B.-E. Sæther, 2011: Climate, icing, and wild arctic reindeer: Past relationships and future prospects. *Ecology*, **92**, 1917–1923, https://doi.org/10.1890/11-0095.1.

——, and Coauthors, 2014: Warmer and wetter winters: Characteristics and implications of an extreme weather event in the high Arctic. *Environ. Res. Lett.*, **9**, 114021, https://doi.org/10.1088/1748-9326/9/11/114021.

Hartmann, D. L., and Coauthors, 2013: Observations: Atmosphere and surface. *Climate Change 2013: The Physical Science Basis*, T. F. Stocker et al., Eds., Cambridge University Press, 159–254.

Il Jeong, D., and L. Sushama 2018: Rain-on-snow events over North America based on two Canadian regional climate models. *Climate Dyn.*, **50**, 303–316, https://doi.org/10.1007/S00382-017-3609-X.

Kohler, J., and R. Aanes, 2004: Effect of winter snow and ground-icing on a Svalbard reindeer population: Results of a simple snowpack model. *Arct. Antarct. Alp. Res.*, **36**, 333–341, https://doi.org/10.1657/1523-0430(2004)036[0333:EOWSAG]2.0.CO;2.

Langlois, A., and Coauthors, 2017: Detection of rain-on-snow (ROS) events and ice layer formation using passive microwave radiometry: A context for Peary caribou habitat in the Canadian Arctic. *Remote Sens. Environ.*, **189**, 84–95, https://doi.org/10.1016/j.rse.2016.11.006.

Littell, J., S. McAfee, and G. Hayward, 2018: Alaska snowpack response to climate change: Statewide snowfall equivalent and snowpack water scenarios. *Water*, **10**, 668, https://doi.org/10.3390/w10050668.

Liu, J., Z. Chen, J. Francis, M. Song, T. Mote, and Y. Hu, 2016: Has Arctic Sea ice loss contributed to increased surface melting of the Greenland ice sheet? *J. Climate*, **29**, 3373–3386, https://doi.org/10.1175/JCLI-D-15-0391.1.

Mason, O. K., D. K. Salmon, and S. L. Ludwig, 1996: The periodicity of storm surges in the Bering Sea from 1898 to 1993, based on newspaper accounts. *Climatic Change*, **34**, 109–123, https://doi.org/10.1007/BF00139256.

Massom, R. A., M. J. Pook, J. C. Comiso, N. Adams, J. Turner, T. Lachlan-Cope, and T. T. Gibson, 2004: Precipitation over the interior East Antarctic Ice Sheet related to midlatitude blocking-high activity. *J. Climate*, **17**, 1914–1928, https://doi.org/10.1175/1520-0442(2004)017<1914:POTIEA>2.0.CO;2.

McCabe, G. J., L. E. Hay, and M. P. Clark, 2007: Rain-on-snow events in the western United States. *Bull. Amer. Meteor. Soc.*, **88**, 319–328, https://doi.org/10.1175/BAMS-88-3-319.

Menne, M. J., I. Durre, R. S. Vose, B. E. Gleason, and T. G. Houston, 2012: An overview of the global historical climatology network-daily database. *J. Atmos. Oceanic Technol.*, **29**, 897–910, https://doi.org/10.1175/JTECH-D-11-00103.1.

Mesquita, M. S., D. E. Atkinson, I. Simmonds, K. Keay, and J. Gottschalck, 2009: New perspectives on the synoptic development of the severe October 1992 Nome storm. *Geophys. Res. Lett.*, **36**, L13808, https://doi.org/10.1029/2009GL038824.

——, ——, and K. I. Hodges, 2010: Characteristics and variability of storm tracks in the North Pacific, Bering Sea, and Alaska. *J. Climate*, **23**, 294–311, https://doi.org/10.1175/2009JCLI3019.1.

Miller, F. L., R. H. Russell, and A. Gunn, 1975: The recent decline of Peary caribou on Western Queen Elizabeth Islands of Artic Canada. *Polarforschung*, **45**, 17–21.

Mundhenk, B. D., E. A. Barnes, E. D. Maloney, and K. M. Nardi, 2016: Modulation of atmospheric rivers near Alaska and the U.S. West Coast by northeast Pacific height anomalies. *J. Geophys. Res. Atmos.*, **121**, 12 751–12 765, https://doi.org/10.1002/2016JD025350.

Pall, P., L. M. Tallaksen, and F. Stordal, 2019: A climatology of rain-on-snow events for Norway. *J. Climate*, **32**, 6995–7016, https://doi.org/10.1175/JCLI-D-18-0529.1.

Pan, C. G., P. B. Kirchner, J. S. Kimball, Y. Kim, and J. Du, 2018: Rain-on-snow events in Alaska, their frequency and distribution from satellite observations. *Environ. Res. Lett.*, **13**, 075004, https://doi.org/10.1088/1748-9326/aac9d3.

Pezza, A. B., J. A. P. Veiga, I. Simmonds, K. Keay, and M. S. Mesquita, 2010: Environmental energetics of an exceptional high-latitude storm. *Atmos. Sci. Lett.*, **11**, 39–45, https://doi.org/10.1002/ASl.253.

Putkonen, J., and G. Roe, 2003: Rain-on-snow events impact soil temperatures and affect ungulate survival. *Geophys. Res. Lett.*, **30**, 1188, https://doi.org/10.1029/2002GL016326.

Reichle, R. H., C. S. Draper, Q. Liu, M. Girotto, S. P. P. Mahanama, R. D. Koster, and G. J. M. De Lannoy, 2017a: Assessment of MERRA-2 land surface hydrology estimates. *J. Climate*, **30**, 2937–2960, https://doi.org/10.1175/JCLI-D-16-0720.1.

——, Q. Liu, R. D. Koster, C. S. Draper, S. P. P. Mahanama, and G. S. Partyka, 2017b: Land surface precipitation in MERRA-2. *J. Climate*, **30**, 1643–1664, https://doi.org/10.1175/JCLI-D-16-0570.1.

Reimers, E., 1982: Winter mortality and population trends of reindeer on Svalbard, Norway. *Arct. Alp. Res.*, **14**, 295–300, https://doi.org/10.2307/1550792.

Rennert, K. J., G. Roe, J. Putkonen, and C. M. Bitz, 2009: Soil thermal and ecological impacts of rain on snow events in the circumpolar Arctic. *J. Climate*, **22**, 2302–2315, https://doi.org/10.1175/2008JCLI2117.1.

Rex, D. F., 1950: Blocking action in the middle troposphere and its effect upon regional climate. *Tellus*, **2**, 275–301, https://doi.org/10.1111/j.2153-3490.1950.tb00339.x.

Semmens, K. A., J. Ramage, A. Bartsch, and G. E. Liston, 2013: Early snowmelt events: Detection, distribution, and significance in a major sub-arctic watershed. *Environ. Res. Lett.*, **8**, 014020, https://doi.org/10.1088/1748-9326/8/1/014020.

Stimberis, J., and C. M. Rubin, 2017: Glide avalanche response to an extreme rain-on-snow event, Snoqualmie Pass, Washington, USA. *J. Glaciol.*, **57**, 468–474, https://doi.org/10.3189/002214311796905686.

Stroeve, J. C., M. C. Serreze, A. Barrett, and D. N. Kindig, 2011: Attribution of recent changes in autumn cyclone associated precipitation in the Arctic. *Tellus*, **63A**, 653–663, https://doi.org/10.1111/j.1600-0870.2011.00515.x.

Wang, D., and Coauthors, 2014: A case study of the November 2012 mixed rain-snow storm over North China. *Acta Meteor. Sin.*, **27**, 601–625, https://doi.org/10.1007/s13351-013-0512-1.

Wernli, H., and C. Schwierz, 2006: Surface cyclones in the ERA-40 dataset (1958-2001). Part I: Novel identification method and global climatology. *J. Atmos. Sci.*, **63**, 2486–2507, https://doi.org/10.1175/JAS3766.1.

Wilson, D. S., D. Pollard, R. M. DeConto, S. S. R. Jamieson, and B. P. Luyendyk, 2013: Initiation of the West Antarctic Ice Sheet and estimates of total Antarctic ice volume in the earliest Oligocene. *Geophys. Res. Lett.*, **40**, 4305–4309, https://doi.org/10.1002/grl.50797.

Ye, H., Y. Daqing, and D. Robinson, 2008: Winter rain on snow and its association with air temperature in northern Eurasia. *Hydrol. Processes*, **22**, 2728–2736, https://doi.org/10.1002/hyp.7094.

Yu, R., Y. Xu, T. Zhou, and J. Li, 2007: Relation between rainfall duration and diurnal variation in the warm season precipitation over central eastern China. *Geophys. Res. Lett.*, **34**, L13703, https://doi.org/10.1029/2007GL030315.